Journal of Crystal Growth 311 (2009) 3563–3567

Contents lists available at ScienceDirect

Journal of Crystal Growth

journal homepage: www.elsevier.com/locate/jcrysgro

Growth of InAsSb/InAs MQWs on GaSb for mid-IR photodetector applications

D. Lackner [a], O.J. Pitts [a,1], S. Najmi [a], P. Sandhu [a], K.L. Kavanagh [a], A. Yang [a], M. Steger [a], M.L.W. Thewalt [a], Y. Wang [b], D.W. McComb [b], C.R. Bolognesi [a,2], S.P. Watkins [a,*]

[a] Department of Physics, Simon Fraser University, Burnaby, BC, Canada V5A 1S6
[b] Department of Materials and London Centre for Nanotechnology, Imperial College London, SW7 2AZ, UK

ARTICLE INFO

Article history:
Received 24 November 2008
Received in revised form
3 April 2009
Accepted 21 April 2009
Communicated by R. Bhat
Available online 5 May 2009

PACS:
68.37.LP

Keywords:
A1. High resolution X-ray diffraction
A1. Interfaces
A3. Organometallic vapor phase epitaxy
A3. Quantum wells
A3. Superlattices
B1. Antimonides

ABSTRACT

We report the OMVPE growth and characterization of InAsSb/InAs strain balanced multiple quantum wells lattice-matched to GaSb substrates for potential application as mid-infrared detectors for wavelengths beyond 4 μm. Detailed transmission electron microscopy measurements were performed to evaluate the degree of Ga and Sb intermixing at the GaSb/InAsSb and InAs/InAsSb interfaces. Photoluminescence emission up to 5 μm was observed for superlattice structures with only 15% antimony. The dependence of PL on wavelength is red shifted compared to expectations based on type I band alignment.

1. Introduction

Antimonide based materials are promising candidates for mid-infrared (2–5 μm) photodiodes [1–4]. Mid-infrared photodiodes (or photodiode-arrays) are of special interest, as most environmentally interesting gases/pollutants show absorption lines or bands (spectroscopic fingerprints) in this region [5,6]. The proposed devices could thus be used for monitoring gases such as CH_4, CO_2, CO, N_2O and O_3 quickly and cost effectively. Further applications could involve thermal imaging (night-vision) and sensors for chemicals of high interest such as explosives. Today's mid-infrared sensors are usually made of HgCdTe alloys, which are difficult to grow and involve the use of Hg vapor as a precursor. A III–V material system is of high interest as a Hg-free material system. Furthermore, previous results indicate that by the appropriate choice of heterojunction barrier layers, some usable response in the mid-IR should be obtainable close to room temperature with this material system [7]. There are challenges when working with antimonides, however, as they only grow with good morphology within a small V:III window [8]. Sb also is known to have a low vapor pressure and thus tends to stick at surfaces, which makes it very effective as surfactant, but often results in a memory effect or segregation.

Most previous reports of photodetector work in this material system involved InAsSb lattice matched to GaSb, having a band gap corresponding to 4.3 μm (0.286 eV) at room temperature [6,7]. In this work we explore the possibility of strain compensated InAs/InAsSb multi-quantum wells (MQW) grown on GaSb substrates by OMVPE. A strain-balanced structure consisting of alternating tensile and compressively strained layers, in which the individual layer thickness is below the critical thickness, permits the use of significantly longer wavelength InAsSb quantum well regions. By stacking several periods of these strain compensated layers, one should be able to achieve sufficient absorption for a photodetector, without generating dislocations. Thus optical absorption considerably beyond the 4.3 μm limit of lattice matched $InAs_{1-x}Sb_x$ should be possible. Due to the predicted type II band alignment, such structures would have an even smaller band gap than either of the constituents [9].

Here we present the growth of strain balanced InAs/InAsSb MQW structures on GaSb substrates. We provide detailed structural characterization using XRD and electron microscopy techniques, which focusses on small but important layer intermixing issues common to antimonide epitaxy. We report PL measurements of

*Corresponding author.
E-mail address: simonw@sfu.ca (S.P. Watkins).
[1] Present address: National Research Council of Canada – Canadian Photonics Fabrication Centre, 1200 Montreal Rd. M-50, Ottawa, Ontario, Canada K1A 0R6.
[2] Currently at Laboratory for Electromagnetic Fields and Microwave Electronics (IfH), ETH Zürich, Gloriastrasse 35, CH-8092 Zürich, Switzerland.

0022-0248/$ - see front matter © 2009 Elsevier B.V. All rights reserved.
doi:10.1016/j.jcrysgro.2009.04.027

these superlattice structures which show that it should be possible to extend the detection wavelength to 5 μm or beyond.

2. Experimental details

The samples were grown by low pressure organometallic vapor phase epitaxy (OMVPE) in a special optical showerhead reactor [10]. Growth was performed on GaSb (0 0 1) substrates miscut 2° towards (1 1 1)B, and also on nominally exact InAs (0 0 1) substrates. To remove the oxide layer on the "epi-ready" GaSb substrates, the wafers were etched for 2 min with concentrated HCl, rinsed in isopropanol and dried under N_2. No treatment was used for the InAs substrates. For growth on GaSb substrates, a GaSb buffer layer was first grown at 540 °C in order to provide a smoother starting surface. The InAsSb/InAs layers were all deposited at a temperature of 500 °C and a pressure of 50 torr. Hydrogen was used as the carrier gas. The precursors were triethylgallium (TEGa) and trimethylindium (TMIn) for the group-III elements and trimethylantimony (TMSb) as well as tertiarybutylarsine (TBAs) for the group-V elements. For the InAsSb structures grown on GaSb (InAs) substrates, the V:III ratio for the InAsSb layers was 5.9 (6.34) and the layers were grown at a rate of 0.75 μm/h (2 μm/h). The distribution coefficient $k = ([Sb]/[As])_{solid}/([Sb]/[As])_{vapor}$ used for the growths varied between 0.4 and 0.5.

The XRD measurements were taken with a Bede D3 high resolution X-ray diffractometer. ω–2θ scans of the (0 0 4) reflection were recorded. Simulations of the structures were fitted to the obtained spectra using the dynamical diffraction simulation program "RADS Mercury" by Bede. In all cases, Sb layer compositions were determined from the fits to the XRD data. The *in situ* optical stress measurement system used was built at Simon Fraser University. The spacing of two parallel beams, created by a solid state laser at 680 nm and an etalon, after being reflected off the wafer, is measured in real time with a CCD camera. The relative spacing of the two beams is proportional to the wafer curvature.

For (scanning) transmission electron microscopy, a FEI field emission Tecnai 20 (200 keV) or a monochromated FEI Titan 80–300 (300 keV) system was used. In scanning mode, a high angle annular dark field (HAADF) detector as well as energy-dispersive X-ray spectroscopy (EDS) was used in order to obtain high resolution compositional information. Cross-section samples were prepared by manual thinning and additional ion-milling with liquid nitrogen cooling at a milling angle of 15°.

A Bomem DA8 Fourier transform spectrometer with a liquid nitrogen cooled InSb photodetector was used to obtain the PL spectra. The samples were mounted strain-free in liquid He at 4.2 K. The PL spectra were collected using a frequency doubled Nd : YVO_4 laser excitation at 532 nm and 200 mW of CW power in a 3 mm diameter spot size.

3. Structural results and discussion

The aim of this work is to demonstrate the growth of approximately strain balanced InAs/$InAs_{1-x}Sb_x$ MQWs on GaSb substrates. For equal layer thickness of InAs and $InAs_{1-x}Sb_x$ this will occur at an Sb mole fraction $x = 0.18$. The layer structure for the samples grown on GaSb substrates is shown in Fig. 1(a). The structures consist of five 20 nm thick compressively strained $InAs_{1-x}Sb_x$ QW layers grown with six 20 nm InAs tensile strained barrier layers. In order to minimize the total strain, 10 nm $InAs_{1-x}Sb_x$ layers were grown at the start and at the end of the stack. Thus, the total number of layers (excluding the GaSb buffer) is 13. For the ideal case of $x = 0.18$, this would result in zero net strain. In fact, our strain compensated MQWs are close to, but not exactly at, the strain balanced condition. Sample 1 achieved an Sb mole fraction of $x = 0.15$ as determined from XRD simulations, which shows a slight net tensile strain in the stack. Samples 2 and 3 achieved an Sb mole fraction of 0.21, which is slightly on the side of compressive net strain. Sample 3 was identical to sample 2 with the exception that the GaSb buffer layer was grown in a separate growth step and cooled to room temperature before the subsequent InAsSb growth. This was done in order to rule out gas phase memory effects, as will be discussed later. The MQW samples discussed in this paper are summarized in Table 1.

The implementation of strain balanced MQWs for optical detectors will require the growth of thick MQW stacks with many layers. *In situ* optical characterization of layer strain will be a very important tool for real time monitoring of the total layer strain during actual device growth. Fig. 1(b) shows the signal of *in situ* optical strain measurements for sample 2 during growth. The wafer curvature is plotted as a function of the growth time, which is proportional to thickness. A positive slope of curvature corresponds to compressive strain in the growing layer (InAsSb) and a negative slope to tensile strain (InAs). The 13 individual layers are resolved in this image including the thin 10 nm layers at the beginning and end of the growth sequence. These

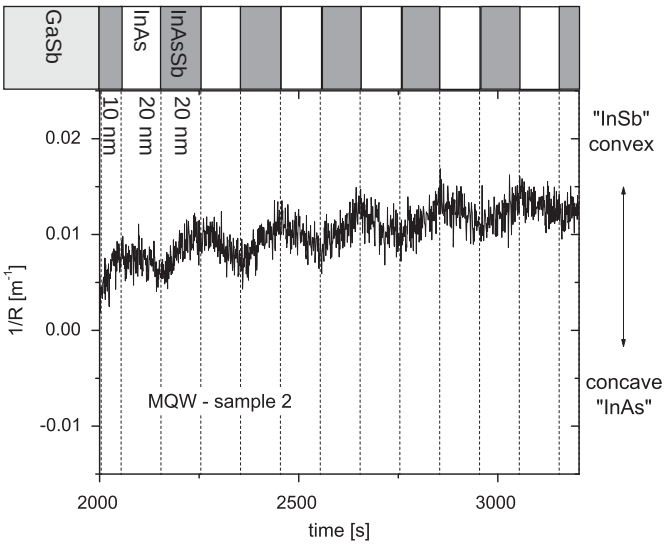

Fig. 1. (a) This shows the layer structure used for the strain balanced InAs/$InAs_{1-x}Sb_x$ MQWs grown on GaSb substrates. All MQW layers are 20 nm except for the first and last InAsSb layers which are 10 nm. (b) *In situ* optical strain measurement monitoring during the growth of sample 2 with $x_{Sb} = 0.21$. The wafer curvature is plotted as a function of growth time. The periodic upward (and downward) slopes are the InAsSb (InAs, respectively) layers. The individual layers are indicated by vertical lines, starting at the first InAsSb layer.

Table 1
MQW samples discussed in the text.

Sample	Substrate	x_{Sb}
1	GaSb[a]	0.15
2	GaSb	0.21
3	GaSb	0.21
4	InAs[a]	0.024
5	InAs[a]	0.07

Sample 3 differed from the other samples in that a GaSb buffer was grown and then the system was cooled to room temperature before reheating for the subsequent growth of the InAsSb/InAs layers.

[a] Denotes samples included in the PL (Fig. 6).

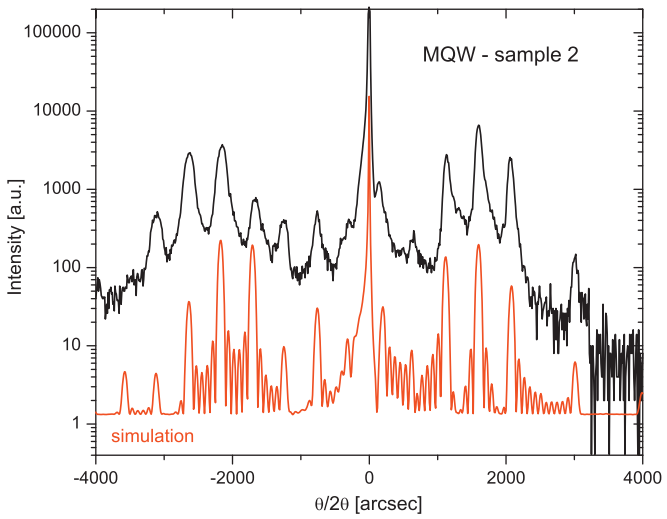

Fig. 2. XRD $\omega-2\theta$ scan of the MQW sample 2 (top) and simulation (bottom). The simulation used an InAsSb layer thickness and composition of 20 nm and $x_{Sb} = 0.21$, respectively. The InAs layer thickness was 19 nm.

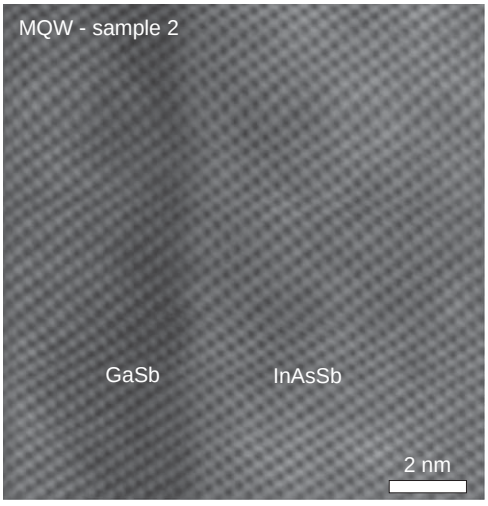

Fig. 3. HAADF-STEM (300 keV) image of the GaSb–InAsSb interface of the first QW of the continuously grown sample 2 along the 1 1 0 direction. The image clearly shows the ordered lattice as well as an absence of dislocations or stacking faults. The slight waviness is due to STEM artifacts.

measurements clearly show the oscillation of the layer strain in real time from compressive (InAsSb) to tensile (InAs) as the growth progresses. The overall rise of the curvature confirms that the total layer structure is under slight residual compressive strain as expected from the XRD data which gave a fitted Sb composition of 21% rather than the target of 18% for perfect strain compensation.

A 0 0 4 XRD scan of the MQW sample 2 is presented in Fig. 2. The fact that satellite peaks are clearly visible and are sharp reveals good overall agreement with the intended structure. In particular, the observation of sharp satellite fringes and thickness fringes rules out appreciable relaxation by dislocation formation. Curve fitting to each spectrum verified the QW thicknesses (20 nm) and the Sb composition in the InAsSb quantum wells ($x_{Sb} = 0.21$). The slight broadening of the measured spectrum compared to the simulation is probably due to Ga and Sb intermixing effects discussed later (see Fig. 4).

The XRD data indicate good but not perfect agreement with the dynamical diffraction simulations based on the intended structures. We performed high resolution TEM in order to further investigate the cause of this remaining discrepancy. The interface between the GaSb and the InAsSb was studied in detail for sample 2. Fig. 3 displays a 300 keV STEM-HAADF image showing contrast predominantly associated with the atomic number differences between the first InAsSb quantum well and the GaSb buffer layer. The interface is planar on an atomic scale with no dislocations or stacking faults evident at the interface. The apparent waviness is due to an artifact of the STEM.

While the STEM image shows the interface to be planar, EDS linescans show that there is some intermixing at the GaSb/InAsSb interface and at the subsequent InAs/InAsSb interfaces. An EDS linescan for sample 2 is shown in Fig. 4. This figure indicates a carryover of Ga into the first InAsSb layer for approximately 6–10 nm. In addition, there is a noticeable asymmetry between the bottom and top interfaces of the InAsSb wells. The bottom InAs/InAsSb interface is abrupt to within the resolution of the EDS measurements (approximately 2.5 nm) while the top InAsSb/InAs interfaces show noticeable grading over a length scale of $\approx$ 10 nm. This is most likely a surface segregation effect and has been reported previously by several groups. The lower surface energy of InSb results in a tendency for Sb rich layers to float on InAs layers, resulting in unintentional Sb incorporation during subsequent InAs growth. This leads to an asymmetry in QW interfaces for materials with large differences in surface energy.

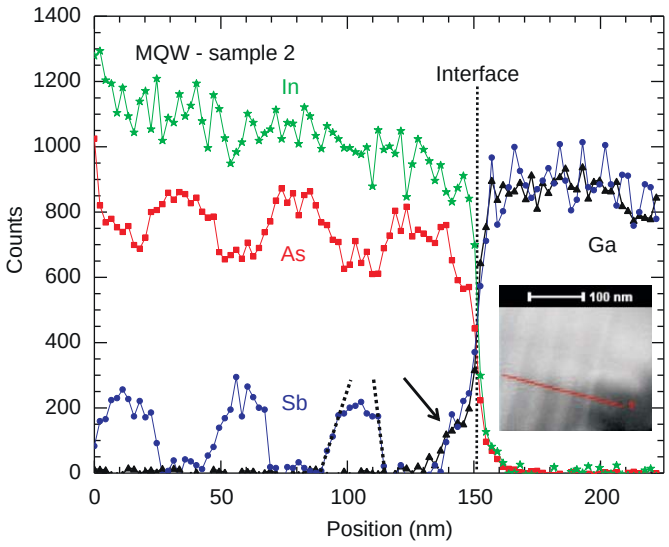

Fig. 4. EDS analysis of the MQW sample 2. The scan was done along the line in the inset (across the GaSb/InAsSb interface perpendicular to the QWs). A plateau of Ga after the interface is clearly seen, as well as an Sb segregation effect indicated by the asymmetric on and off behavior of the quantum wells. The change of the In signal level with position is due to the gradual change in sample thickness.

The Ga memory effect observed here has not been reported to our knowledge. There are a couple of possible reasons for it: (1) carryover of Ga from the pipework following gas switching between the GaSb and InAsSb layers growths and (2) carryover of Ga adsorbed on the sample holder (susceptor). In order to distinguish between these two possibilities, we grew an additional sample 3 with $x_{Sb} = 0.21$ by a two-step procedure in which the GaSb buffer layer was grown, and the sample was then cooled to room temperature in order to completely purge the gas lines. The InAsSb/InAs MQW layers were then grown under conditions in which there could be no Ga gas phase memory effects. EDS data for sample 3 were very similar to that of the continuously grown sample 2, verifying that the cause of the Ga carryover was not due to gas switching effects.

TEM measurements of the $x = 0.21$ MQW samples 2 and 3 were obtained under both 0 0 4 and 2 2 0 diffraction conditions. Fig. 5 shows results for sample 3. Similar images were obtained

for sample 2. Using 0 0 4 bright field (BF) conditions at 200 keV (Fig. 5a) the QWs appear to be smooth with sharp interfaces and constant thickness in agreement with results from the XRD simulations. When studying the same interface with a TEM under 220-bright field conditions (Fig. 5b), which is a reflection that is much more sensitive to strain, lateral strain fluctuations were detected. The strain fields have a mean lateral distance of ≈ 5 nm and reach about 20 nm into the InAsSb/InAs. The strain fields are detected in the two-step growth sample (3) as well as the continuously grown one (2). Similar results were obtained for an InAsSb sample lattice matched to GaSb. The most likely cause of these strain fluctuations is the Ga carryover observed in Fig. 4 since they have a similar length scale as the Ga memory observed in EDS. We have shown that the carryover does not originate from nonideal gas switching. It is most likely that it originates from Ga adsorbed on the susceptor.

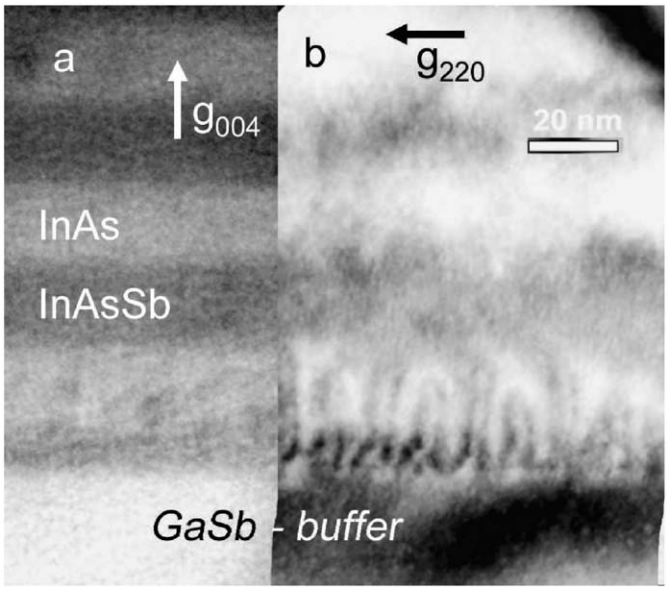

Fig. 5. Bright field TEM images of the start of the two-step growth MQW structure (sample 3) for diffraction conditions: (a) (0 0 4) and (b) (2 2 0). The GaSb buffer and the first MQW layers (starting with a 1/2-layer of InAsSb) are shown. The strong contrast fluctuations are due to lateral strain fluctuations that originate at the GaSb–InAsSb interface. The scale marker is identical for both images.

We have also grown MQW structures on InAs substrates at lower Sb compositions for PL measurements. These samples consisted of 3 $InAs_{1-x}Sb_x$ QWs sandwiched between InAs barriers. The thicknesses of the InAs and InAsSb layers were also set to 20 nm as for the growth on GaSb substrates. Since these are not strained balanced structures, the number of wells was reduced compared with the samples on GaSb substrates in order to minimize the total layer strain, and avoid dislocation formation. The Sb compositions of the $InAs_{1-x}Sb_x$ layers of the MQW structures grown on GaSb and InAs substrates are summarized in Table 1.

4. Optical results and discussion

Fig. 6 shows the PL peak energy at 4.2 K as a function of Sb composition for various samples. Three basic groups of samples are shown: (1) thick (>100 nm) InAsSb samples grown on GaSb substrates close to the lattice matched condition, $x_{Sb} = 0.09$, (2) $InAs/InAs_{1-x}Sb_x$ MQWs grown on InAs substrates, and (3) a $InAs/InAs_{1-x}Sb_x$ MQW grown on a GaSb substrate.

The experimental PL energies are compared to the calculated band gap of unstrained InAsSb (solid line) [12]. The calculated strained band gap (E_c–E_{hh}) in the case of InAsSb grown on GaSb (InAs) substrates is plotted as a dashed (dotted) line. The change of the band gap with strain was calculated using the procedure described by Marzin et al. [13] with the assumption of linearly varying elastic constants taken from Levinstein and Rumanyantsev [14]. The calculated curve does not include possible effects of quantum size shifts, due to the lack of literature data on the band offsets. The calculated energies are therefore lower limits. The thick InAsSb samples (□, △) show PL energies which average about 10 meV lower than the calculated energy gap, which is consistent with free-to-bound or donor–acceptor pair transitions.

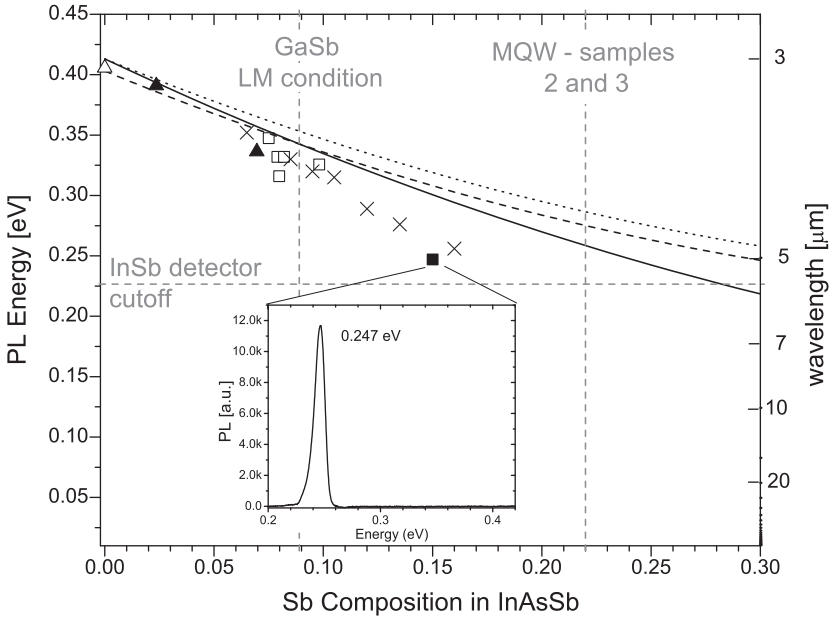

Fig. 6. PL peak energy as a function of Sb content in InAsSb at 4.2 K. Thick (>100 nm) InAsSb samples on GaSb substrates (□), an InAs substrate (△), strain compensated MQW samples on a GaSb substrate (■) and on InAs substrates (▲) are plotted in comparison to the unstrained band gap (solid line), as well as the energy gap between the conduction band and the heavy hole band when strained on InAs (dotted line) and on GaSb (dashed line). Previously reported InAs/InAsSb MQW structures from Liu et al. [11] are included (×). The inset shows the recorded spectrum of the InAsSb/InAs MQW sample grown on GaSb.

The strain balanced MQW sample grown on a GaSb substrate (sample 1) with $InAs_{0.85}Sb_{0.15}$ shows an emission energy of 0.247 eV (5.02 μm) which is 61 meV below the calculated strained band gap of InAsSb. This is too large to be due solely to shallow impurity effects, such as donor–acceptor-pair or free-bound transitions. The finding of the lowered energy has also been recently reported in the literature by Liu et al. [11], who studied InAsSb/InAs MQWs on InAs substrates for various Sb compositions with a quantum well thickness of 7 nm. These data are also included in Fig. 6 (×). Whether the lowered energy is explained by the predicted type II band alignment, or has other causes like a possible ordering effect or compositional fluctuations needs to be clarified, as contradictory results are found in the literature. *Ab initio* calculations [9] predict a type IIb (binary) alignment of biaxially compressively strained InAsSb on unstrained InAs, in which the transition occurs from the InAs conduction band to the InAsSb valence band. However, different authors have reported contrary results from magneto-optical measurements for type IIa [15] (alloy) alignment, in which the transition occurs from the InAsSb conduction band to the InAs valence band. Other workers indicate evidence for type I band alignments [16].

Note that PL was not detected from samples 2 and 3 with $x_{Sb} = 0.21$. If we extrapolate a straight line through the three MQW samples in Fig. 6, the energy of samples 2 and 3 would lie at 0.19 eV, about 40 meV below the detection window of the InSb detector used with our PL setup.

5. Conclusions

We have reported the OMVPE growth of $InAs_{1-x}Sb_x/InAs$ MQW structures on GaSb substrates with x in the range 0.15–0.21. Detailed XRD and electron microscopy measurements indicate good overall structural quality, but with some evidence of Ga and Sb memory effects attributed to susceptor carryover and surface segregation. PL emission of 5.02 μm for a strain balanced MQW with $x_{Sb} = 0.15$ has been reported. The PL peak energy was found to be approximately 60 meV below the expected strained band gap of $InAs_{0.85}Sb_{0.15}$. The PL results reported here support the concept of an InAsSb/InAs strain balanced superlattice structure for optical detection beyond 5 μm.

Acknowledgments

The authors acknowledge the support of the Natural Sciences and Engineering Research Council of Canada and Perkin Elmer Optoelectronics, Vaudreuil, Quebec. D.W. McComb would like to thank the Engineering and Physical Sciences Research Council for funding for the Titan facility at Imperial College London (EP/C51596X).

References

[1] R. Triboulet, Semicond. Sci. Technol. 5 (1990) 1073.
[2] H. Shao, W. Li, A. Torfi, D. Moscicka, W.I. Wang, IEEE Photonic. Tech. L. 18 (2006) 1756.
[3] A. Rakovska, V. Berger, X. Marcadet, B. Vinter, G. Glastre, T. Oksenhendler, D. Kaplan, Appl. Phys. Lett. 77 (2000) 397.
[4] Y. Paltiel, A. Sher, A. Raizman, D. Majer, A. Arbel, A. Feingold, J. Levy, R. Naaman, IEEE Sens. J. 6 (2006) 1195.
[5] V. Vankova, P. Gladkov, J. Botha, J. Cryst. Growth 275 (2005) 1109.
[6] A. Rakovska, V. Berger, X. Marcadet, B. Vinter, K. Bouzehouane, D. Kaplan, Semicond. Sci. Technol. 15 (2000) 34.
[7] G. Marre, B. Vinter, V. Berger, Semicond. Sci. Technol. 18 (2003) 284.
[8] R.M. Biefeld, Mat. Sci. & Eng. R 36 (2002) 105.
[9] S.H. Wei, A. Zunger, Phys. Rev. B 52 (1995) 12039.
[10] Y. Guo, O.J. Pitts, W.Y. Jiang, S.P. Watkins, J. Cryst. Growth 297 (2006) 345.
[11] P.-W. Liu, G. Tsai, H.H. Lin, A. Krier, Q.D. Zhuang, M. Stone, Appl. Phys. Lett. 89 (2006) 201115.
[12] Z.M. Fang, K.Y. Ma, D.H. Jaw, R.M. Cohen, G.B. Stringfellow, J. Appl. Phys. 67 (1990) 7034.
[13] J. Marzin, J. Gerard, P. Voisin, J. Brum, Semiconductors and Semimetals, Strained-Layer Superlattices: Physics, vol. 32, Academic Press, New York, 1990.
[14] M.S.M. Levinstein, S. Rumanyantsev (Eds.), Handbook Series on Semiconductor Parameters, vols. 1 and 2, World Scientific, London, 1999.
[15] Y.B. Li, D.J. Bain, L. Hart, M. Livingstone, C.M. Ciesla, M.J. Pullin, P.J.P. Tang, W.T. Yuen, I. Galbraith, C.C. Phillips, C.R. Pidgeon, R.A. Stradling, Phys. Rev. B 55 (1997) 4589.
[16] S.R. Kurtz, R.M. Biefeld, Appl. Phys. Lett. 66 (1995) 364.